



Weldability and shear strength feasibility study for automotive electric vehicle battery tab interconnects

Abhishek Das¹ · Dezhi Li¹ · David Williams¹ · David Greenwood¹

Received: 4 July 2018 / Accepted: 13 December 2018 / Published online: 3 January 2019
© The Author(s) 2019

Abstract

Lithium-ion-based secondary battery packs are emerging as an alternative power source and are being increasingly used in electric vehicles, hybrid or plug-in hybrid electric vehicles. Typically, a standard automotive battery pack consists of hundreds, even thousands, of individual cells which are connected in series and/or parallel to deliver the required power and capacity. There is an increasing need for manufacturing of battery packs to meet the demand reflecting the uptake of these vehicles. This triggers the need for suitable joining methods which will provide mechanical strength on a par with electrical and thermal characteristics. This work focuses on characterisation of shear strength of battery tab-to-tab joints for both similar and dissimilar materials by using combinations of aluminium (Al) and nickel-coated copper (Cu[Ni]) tabs. The joining techniques with application for battery tab interconnects are ultrasonic metal welding, resistance spot welding and pulsed TIG spot welding. Lap shear and T-peel tests are performed to evaluate the joint strength. In general, lap shear strength is four to seven times higher than the T-peel strength obtained from all three joining methods. In addition, an indicator is developed in this paper based on lap shear-to-T-peel strength reduction ratio which provides additional information on joint strength characteristics, and subsequently, it can be used as a threshold by quality engineers for an indication on selection of joining methods having an acceptable strength reduction ratio.

Keywords Automotive battery · Tab interconnects · Joint strength · Ultrasonic metal welding · Pulsed TIG spot welding · Resistance spot welding

1 Introduction

Vehicles running on fossil fuels are one of the main contributors to greenhouse gas emissions. In Europe, it has been reported that 12% of total emissions of carbon dioxide (CO₂), the main greenhouse gas, are generated by automotive vehicles [1]. Stringent emission targets are set to reduce greenhouse gas generation for all surface transport vehicles, especially for automobiles [2]. Towards meeting this target, electric vehicles (EVs), hybrid electric vehicles (HEVs) and plug-in hybrid electric vehicles (PHEVs) are emerging. Typically, an electric vehicle battery pack is organised with a hierarchical structure consisting of individual cells, modules and pack. A typical automotive application is illustrated in

Fig. 1 showing the battery pack position within an EV, the battery pack and the stacking pattern of individual cells in a module together with ancillary components. To deliver power and driving range, a large number of cells have to be connected by appropriate joining techniques. For example, in a pouch cell-based battery module, cell-to-cell electrical interconnects are achieved with tab-to-tab or tab-to-busbar joints. In the pouch cell-based module design, positive and negative terminal tabs are positioned either at opposite ends or at the same end of the cell based on series or parallel connection requirements [3]. Therefore, the cells are joined either by tab-to-tab or tab-to-busbar connections as shown in Fig. 2. Making these tab joints involves several challenges, including (i) joining of multiple, thin, dissimilar materials of varying thicknesses, (ii) highly conductive and reflective surfaces, (iii) potential damage (thermal, mechanical or vibrational) during joining and (iv) joint durability. Hence, there is a need for suitable joining techniques to support diverse joining requirements during battery pack manufacture.

Technical Editor: Márcio Bacci da Silva, Ph.D.

✉ Abhishek Das
A.Das.1@warwick.ac.uk

¹ WMG, The University of Warwick, Coventry CV4 7AL, UK

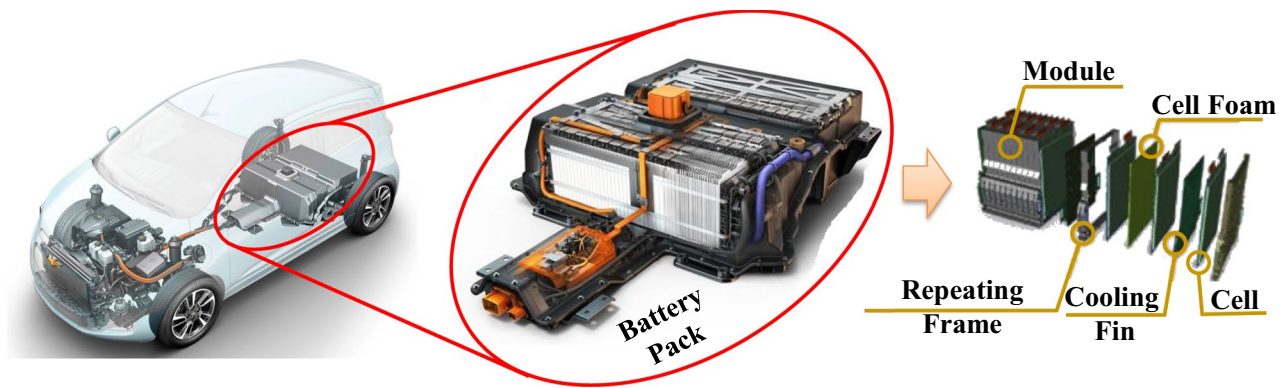


Fig. 1 An illustration of the battery pack and schematic of stacking pattern composed of cells and ancillary components (adapted from Chevrolet Spark EV battery pack) [4, 5]

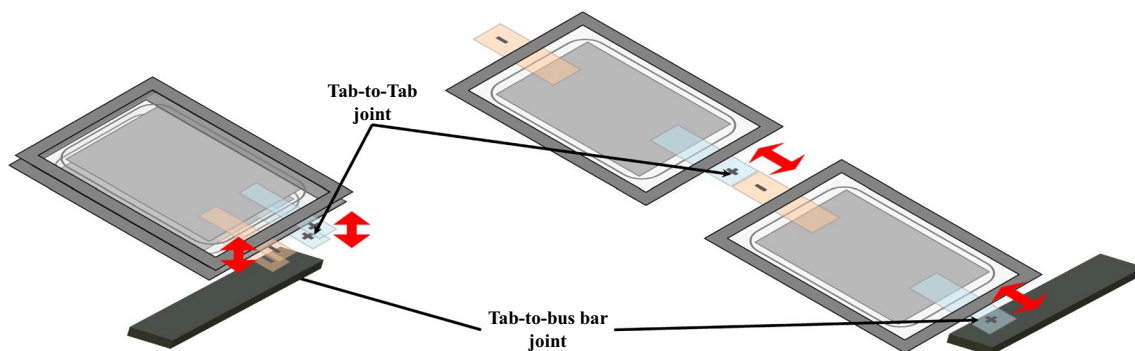


Fig. 2 An illustration of tab-to-tab and tab-to-busbar joints made during pouch cell-based module manufacture

As automotive vehicles are often exposed to adverse thermal and impulse conditions, it is necessary to produce reliable and durable battery interconnects. Comprehensive research has been undertaken focusing on Li-ion battery chemistry, power capacity improvements, performance enhancements or battery testing and characterisation [6–8]. However, there is a lack of information available on the joint strength of battery interconnects. Therefore, detailed studies are required on joining methods, and subsequently, their influence on joint strength.

1.1 Overview of joining methods

Suitable joining methods for pouch cell tab-to-tab interconnects, such as ultrasonic metal welding, resistance spot welding and pulsed TIG spot welding [9, 10], are selected as candidate methods for this feasibility study. The advantages, disadvantages and challenges of these joining methods are summarised in Table 1.

Ultrasonic metal welding (UMW) is a solid-state welding process where electrical energy is converted into high-frequency mechanical vibration to generate heat between joining surfaces [11, 12] with a maximum

process temperature normally 0.3 to 0.5 times that of the absolute melting temperature of the substrate materials. The UMW system and working principle are illustrated in Fig. 3. Ultrasonic energy is used to produce oscillating shear to create solid-state bonds between two sheets clamped under pressure [13, 14]. UMW is considered to be the best process when welding multiple thin sheets and dissimilar materials that typically produce brittle alloys at the weld area [15, 16]. Due to these favourable conditions, UMW is considered a superior process for tab-to-tab and tab-to-busbar joining [17, 18].

Resistance spot welding (RSW) works on the principle of electrical resistance at the mating surfaces creating localised heating and fusion of materials under pressure when a high current passes through them [20–22]. Figure 4 provides a schematic illustration of resistance spot welding used for tab welding. In spite of good quality control characteristics and easy automation, RSW has many challenges when applied to battery welding due to RSW electrode sticking (i.e. pickup of material on the electrode tips) [23], dissimilar materials having different melting temperatures and the smaller weld nugget concentrating current flow and creating heat during charging–discharging of the cell [9]. There are limited

Table 1 Summary of battery tab welding methods

Joining method	Advantages	Disadvantages	Challenges
Ultrasonic metal welding [9, 10, 17, 26]	<ul style="list-style-type: none"> • Solid-state welding process • Able to join dissimilar materials of different melting points • Able to weld thin sheets with thick plates • Good for highly conductive and reflective materials • Multiple sheets/stack-ups of varying thicknesses • High mechanical strength and low electrical resistance • No need for fluxes, filler materials or protective gases • Surface preparation not critical 	<ul style="list-style-type: none"> • Mainly suitable for pouch cells tab-to-tab or tab-to-busbar • Two-sided access required • Restricted to material thickness (up to 3 mm for aluminium and 1 mm for harder materials) • Difficult to join high strength and hard materials • Possibility of sonotrode sticking • High surface deformation and indentation 	<ul style="list-style-type: none"> • Access of anvil and sonotrode: change of geometry, design for specific application required • Improper design may damage the pouch cell due to ultrasonic vibration • Proper selection of process parameters to avoid sonotrode sticking
Resistance spot welding [9, 10, 27]	<ul style="list-style-type: none"> • Low-cost joining process • Good quality control and joint monitoring • Easy automation for industrial production application • No need for fluxes, filler materials or protective gases 	<ul style="list-style-type: none"> • Difficult for highly conductive and dissimilar materials • Surface cleaning of contaminants, (i.e. grease, oil and dirt) • RSW electrode sticking with material • Additional process and maintenance for RSW electrode tip dressing 	<ul style="list-style-type: none"> • Difficult to produce larger nugget • Joining of more than two layers • Weld parameter selection to reduce possible expulsions • Electrode force control and current control to produce uniform joint
Pulsed TIG spot welding [10, 25, 28, 29]	<ul style="list-style-type: none"> • Low-cost fusion type welding process • High joint strength and low resistance • No need for filler wire, unlike traditional TIG welding • Able to join dissimilar materials • Good for conductive and reflective materials • Easy automation for industrial application 	<ul style="list-style-type: none"> • High thermal input and potential heat-affected zone • Possibility of porous joints • Requirement for inert gas shielding • Quality control and monitoring techniques required 	<ul style="list-style-type: none"> • Crucial to control arc welding parameters to avoid possible overheating • Difficult to join Al due to oxide layer (AC pulsed TIG spot welding more suitable) • Difficult to joint more than two layers

published data on the application of RSW to the manufacture of battery systems for the major electric vehicles.

Pulsed TIG spot welding utilises a non-consumable tungsten electrode and shielding gas to produce a pulsed TIG arc without filler wire to join thin materials by localised fusion [24]. Figure 5 illustrates the welding system including welding principle and experimental set-up. The arc pulse has a very short duration, in the tens of milliseconds, with reduced heat input; however, it is still crucial to control the welding parameters to avoid overheating of the battery cell and creation of a larger heat-affected zone [25]. There is limited information on the application of pulsed TIG spot welding for joining of existing electric or hybrid vehicle battery packs.

1.2 Overview of joint strength evaluation

Lap shear and T-peel tests are performed to evaluate the strength of similar and dissimilar material joint configurations. When individual joint strength (i.e. lap shear or

T-peel) satisfies the target value set by quality engineers for each joining method and stack-up, a lap shear-to-T-peel joint strength ratio can provide additional information for selecting a specific joining technology. In this paper, a strength reduction ratio has been defined by considering the ratio of the difference between lap shear and T-peel strengths, to the lap shear strength (as defined in Eq. 1) for the same experimental conditions and stack-up. By modifying the process parameters when an incremental increase in lap shear strength was observed, the corresponding T-peel strength was normally found to increase for an identical stack-up and the same joining method. However, the rate of increase for lap shear strength and T-peel strength is different (see Fig. 6). This rule was observed in our study and is also demonstrated in research conducted by Han et al. [30]. Considering the positive correlation between lap shear and T-peel, the value of the strength reduction ratio will become closer to 1, but will never reach this value, as process conditions are altered to

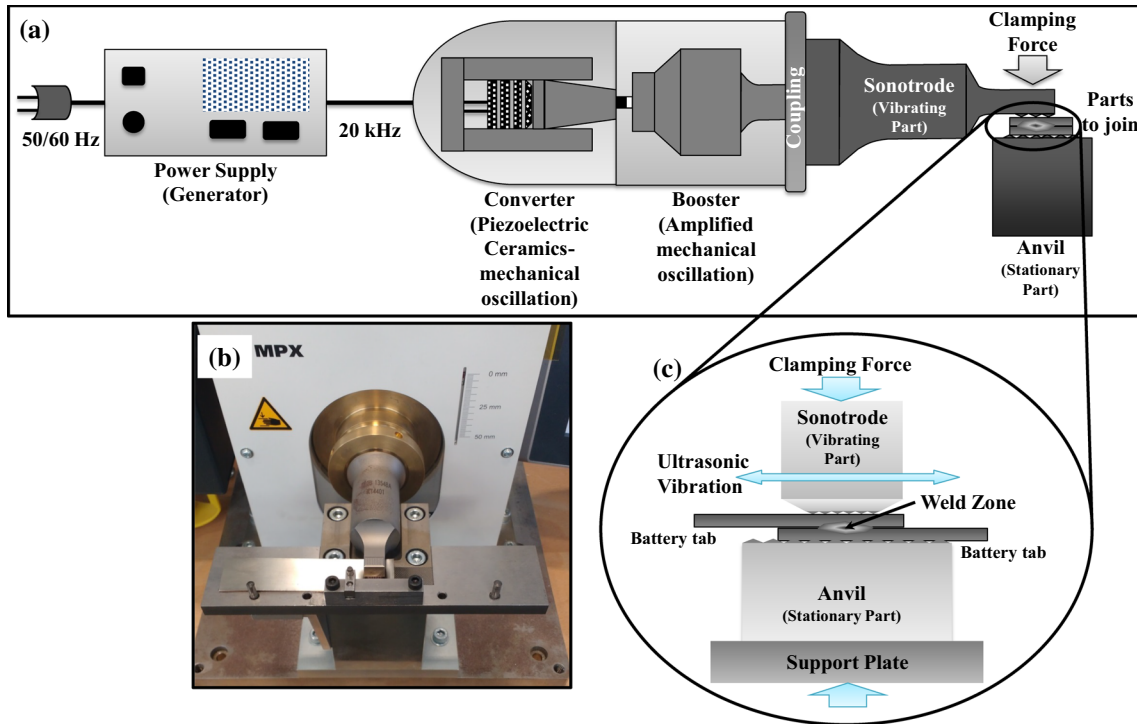
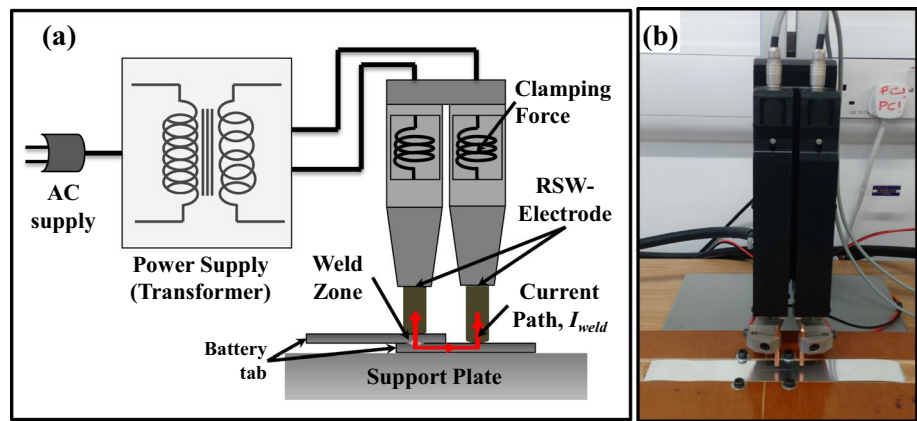


Fig. 3 An illustration of ultrasonic metal welding **a** schematic diagram of welding system [19], **b** battery tab joining set-up, and **c** expanded illustration of welding principle [14]

Fig. 4 An illustration of RSW **a** schematic of welding system, and **b** tab joining set-up



improve joint strength. Therefore, it can be considered that a higher strength reduction ratio indicates stronger joints.

$$\begin{aligned}
 \text{Strength Reduction Ratio} &= \frac{\text{Lap shear strength} - \text{T - peel strength}}{\text{Lap shear strength}} \\
 &= 1 - \frac{\text{T - peel strength}}{\text{Lap shear strength}}
 \end{aligned}
 \tag{1}$$

Further, the strength reduction ratio is independent of joint size (e.g. nugget size) as it considers identical experimental conditions and stack-up. When joints produced by various joining methods satisfy the lower acceptable strength

criteria (i.e. joint strength \geq target value), then all the joining methods are qualified to produce joints with satisfactory strengths; however, they may have different absolute joint strengths due to different weld nugget sizes. Therefore, one way to compare joint strength produced using different joining processes is to evaluate strength per unit area. However, obtaining accurate nugget size is not trivial and involves detailed metallographic inspection. Additionally, often it is difficult to obtain joint area accurately when the joint is made in the form of linear or circular seams/joints. Under these circumstances, the strength reduction ratio can provide useful information for comparing joint strength made

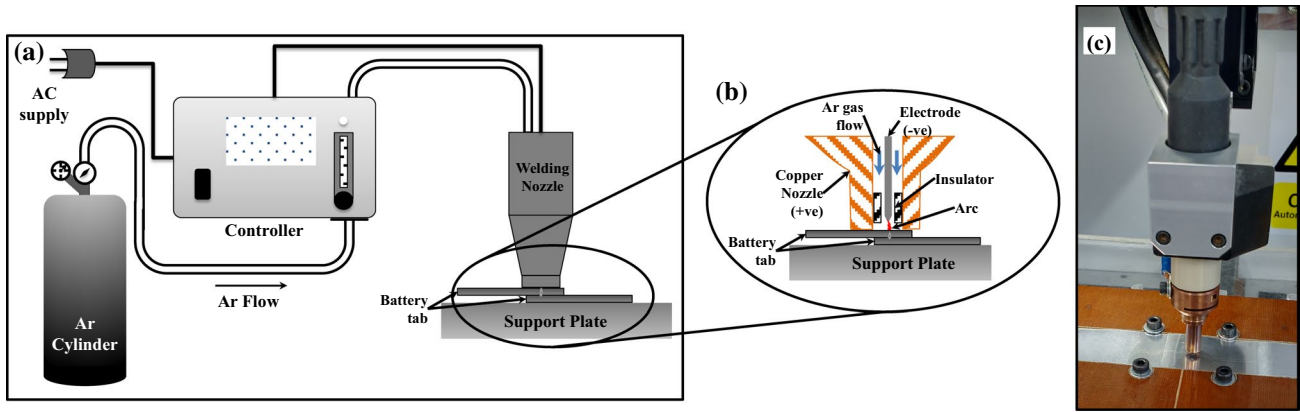


Fig. 5 An illustration of pulsed TIG spot welding a schematic of welding system, b cross-sectional view of tab joining set-up, and c experimental set-up

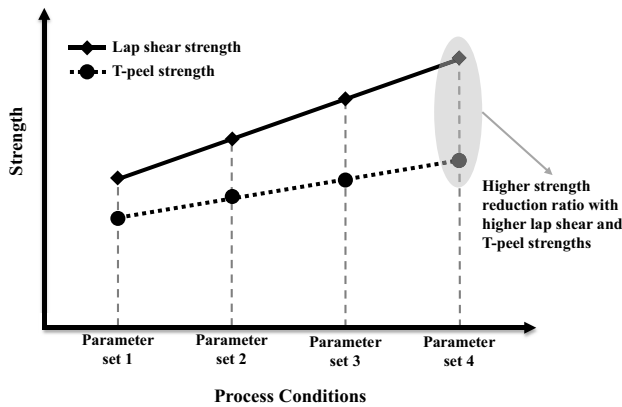
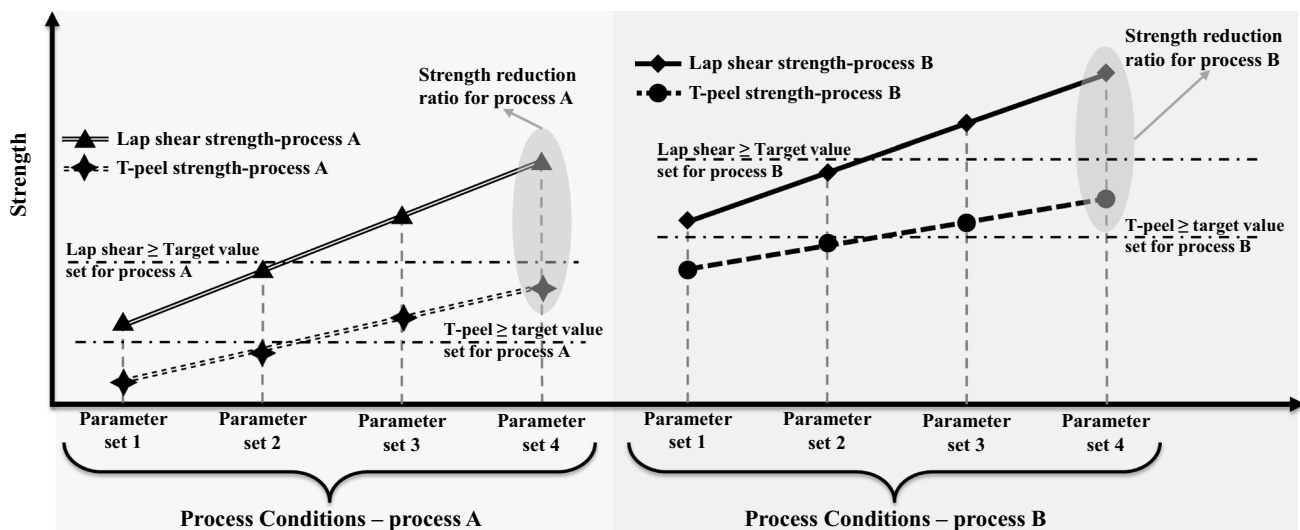


Fig. 6 An illustration of rate of change for the lap shear and T-peel strengths with respect to process conditions

by different joining processes as it is independent of nugget size. For example, Fig. 7 illustrates the lap shear and T-peel strengths of two different processes (i.e. ‘process A’ and ‘process B’) and they both satisfy the acceptable strength criteria (e.g. process parameter set 3 and 4 for process A and B). Although the absolute strengths for ‘process A’ are lower than that of ‘process B’, the strength reduction ratio of ‘process A’ is higher which implies that the ‘process A’ produces superior joints compared to ‘process B’ in terms of joint strength. In the case of different joining processes having the same strength reduction ratio but different absolute strengths, the joining process can be considered as comparable/equivalent in terms of joint strength. Subsequently, joints with different nugget sizes made by different joining processes can be compared using the strength reduction ratio,



Strength reduction ratio of process A > Strength reduction ratio of process B

Fig. 7 An illustration of strength comparison based on strength reduction ratio between two different processes

and further, can be used to assist the selection of candidate joining method.

There is limited literature available on joint strengths using the aforementioned three joining methods. Therefore, the scope of this paper is to investigate the feasibility of the joining processes and then, focus on bridging the identified gaps by characterising shear strength. The joint quality indicator introduced in this paper, i.e. strength reduction ratio, provides additional information on strength behaviour produced by different joining methods. When various joining methods produce joints with acceptable lap shear and T-peel strength criteria (i.e. joint strength \geq target value), then the strength reduction ratio is useful to select specific joining method. However, metallographic inspection is unavoidable when detailed investigations are required to identify the in-depth behavioural phenomena. As the main focus of the paper is the feasibility study based on shear strength, detailed metallographic inspections (e.g. characterisation of penetration, interface width of joint or hardness testing) of joints produced by the joining methods are not within the scope of the present paper.

The remainder of the paper is arranged as follows: Sect. 2 describes the experimental investigation approach adopted

in this study, followed by results and discussions in Sect. 3; and Sect. 4 brings out the conclusions and final remarks.

2 Experimental details

The following sections describe materials used for experimentation, preparation of test samples, test conditions and selection of process parameters for ultrasonic, resistance spot and pulsed TIG spot welding.

2.1 Materials, test specimens and test conditions

As the primary objective of this work is to evaluate joint strength, the materials, stack-up combinations and process parameters are chosen to represent a battery tab-to-tab production application. The most commonly used tab materials, especially for pouch cell tab-to-tab connection application, are either aluminium (Al) or nickel-coated copper (Cu[Ni]). Commercially available and production representative tab materials, listed in Table 2, are used to produce specimens for lap shear and T-peel tests in the combinations detailed in Tables 4, 5 and 7. Schematic diagrams of lap shear and T-peel samples are shown in Fig. 8. Lap shear and T-peel specimens were prepared, as illustrated in Fig. 8, using ultrasonic metal welding, resistance spot welding and pulsed TIG spot welding. Each test variant was repeated four times, and the average of the four replicates was used for analyses. Lap shear and T-peel tests were carried out using an Instron 5800 test frame with a 100-kN load capacity. As the expected loads from lap shear and T-peel tests are quite low, a 1-kN load cell was used to measure the joint strength for better resolution. Lap shear and T-peel tests were performed using

Table 2 Tab materials used for experimental investigations

Tab material	Material specification	Nominal thickness (mm)
Aluminium, Al	AW1050A-H18, BS EN546	0.2 and 0.3
Copper–Nickel-coated, Cu[Ni]	CW004A-H040, BS EN1652 (C101SI BS2870)	0.2 and 0.3

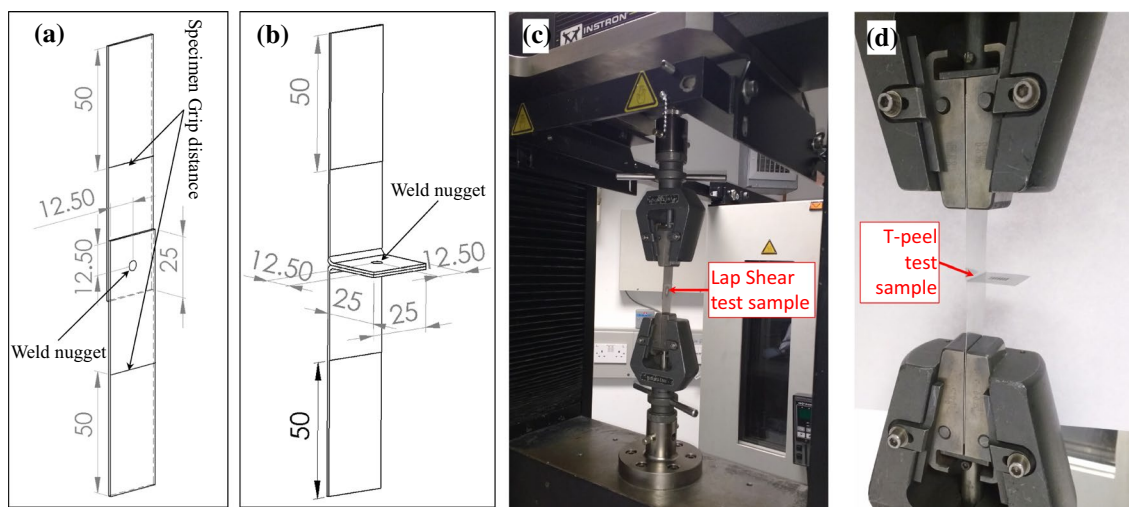


Fig. 8 Test specimens and set-up **a** schematic diagram of lap shear specimen, **b** schematic diagram of T-peel specimen, **c** test set-up for lap shear specimen with test frame, and **d** test set-up for T-peel specimen (enhanced view of test grips)

cross-head speeds of 2 mm/min and 20 mm/min, respectively. Both test variants are illustrated in Fig. 8.

2.2 Process parameter selection

Pilot tests were conducted to identify the process window and suitable joining parameters for each joining method. Based on the pilot experimental results, joining parameters were selected for producing the welds. The following sections describe the details of the process parameters used for producing the different joint configurations.

2.2.1 Ultrasonic metal welding

Ultrasonic metal welding was conducted using welding energy as the main controlling parameter where ultrasonic operation remained active until the target energy was reached. When welding in constant welding energy mode, the welding time varies slightly and depends primarily on the welding pressure and amplitude. It was also observed that when welding dissimilar materials, Cu[Ni] and Al, Cu[Ni] was preferred as the upper sheet and Al as the lower sheet as this combination gave a better result. The sonotrode used for this application can create ultrasonic welds of $10 \times 6 \text{ mm}^2$ area. The amplitude for the ultrasonic vibration was kept constant at 80% of the coded value (100% peak-to-peak amplitude corresponds to 60 μm) and the working

pressure held at 2.5 bar. The trigger mode time was set at 0.2 s which allowed converting of the traversing pressure to welding pressure. Tables 3 and 4 summarise the constant and key controlling process parameters used for welding the various stack-up combinations, respectively.

2.2.2 Resistance spot welding

In general, resistance spot welding is effective when the joining process is controlled by the current passing between the joining interfaces. Similar to ultrasonic metal welding, certain parameters were kept constant and the current was used as the main variable parameter during resistance spot welding. Copper-to-copper and copper-to-aluminium welding was conducted using tungsten electrodes of diameter 3.2 mm, and aluminium-to-aluminium welding was performed using the copper electrodes of the same diameter. A typical single-pulse spot welding cycle consists of five segments which are: squeeze time before applying any current, current rise time to allow the current to reach peak, peak time to allow the welding at allowable peak current, fall time to allow the current to decrease and hold time to hold the specimen after welding. A dual-pulse spot welding cycle consists of the above five segments and one additional which is dwell time (i.e. the time allowed between two consecutive current pulses). For all the test combinations in these experimental investigations, squeeze time, rise time, fall time and hold time were kept at 400 ms, 10 ms, 10 ms and 300 ms, respectively, as they have minor effects on the weld strength. Only peak current and peak current application time were varied to obtain satisfactory welds. Table 5 summarises the process parameters used for welding of different stack-up combinations. It was observed during dissimilar materials joining that Cu[Ni]-to-Al was preferable and produced comparatively strong welds compared to Al-to-Cu[Ni]. Further, joining of 0.3 mm Cu[Ni]-to-Cu[Ni] was challenging due to high electrical conductivity (i.e. low electrical resistance), requiring a dual pulse, and a single-pulse type was used for all other combinations.

Table 3 Constant parameters during joining of tab materials using ultrasonic metal welding

Parameter	Value
Working pressure	2.5 bar
Ultrasonic frequency	20 kHz
Amplitude	80%
Peak-to-peak amplitude	60 μm
Holding pressure after welding	2.0 bar
Holding time after welding	0.3 s
Joining area	$10 \times 6 \text{ mm}^2$

Table 4 Key controlling parameters during joining of tab materials using ultrasonic metal welding

Stack-up combination				Controlling parameter	Value (Ws)	Suitable range (Ws)
Upper material	Thick-ness (mm)	Lower material	Thick-ness (mm)			
Al	0.2	Al	0.2	Energy	60	30–120
Al	0.3	Al	0.3	Energy	60	30–120
Cu[Ni]	0.2	Cu[Ni]	0.2	Energy	1500	1000–2500
Cu[Ni]	0.3	Cu[Ni]	0.3	Energy	1500	1000–2500
Cu[Ni]	0.2	Al	0.2	Energy	380	200–560
Cu[Ni]	0.3	Al	0.3	Energy	380	200–560

Table 5 Combination of process parameters used for joining tab materials using resistance spot welding

Stack-up combination				Process parameters					
Upper material	Thick-ness (mm)	Lower material	Thick-ness (mm)	Pulse type	Peak current (A)		Peak time (ms)		Dwell time (ms)
					Value	Suitable range	Value	Suitable range	
Al	0.2	Al	0.2	Single	2600	2000–3000	30	25–35	N/A
Al	0.3	Al	0.3	Single	2900	2800–3000	40	35–45	N/A
Cu[Ni]	0.2	Cu[Ni]	0.2	Single	3400	3300–3500	30	25–35	N/A
Cu[Ni]	0.3	Cu[Ni]	0.3	Double	3850	3700–3900	30	25–35	10
Cu[Ni]	0.2	Al	0.2	Single	2650	2500–2700	25	20–35	N/A
Cu[Ni]	0.3	Al	0.3	Single	3000	2900–3100	30	25–35	N/A

Table 6 Constant parameters during joining of tab materials using pulsed TIG spot welding

Parameter	Value
Argon flow rate	3 l/min
Nozzle diameter	7 mm
Electrode	Tungsten
Electrode diameter	1.6 mm
Up-slope time	1 ms
Down slop time	30 ms

2.2.3 Pulsed TIG spot welding

Pulsed TIG spot, or micro-TIG, welding was conducted by controlling the peak current and pulse duration under an inert gas environment. A micro-TIG pulse is composed of three stages which are: up-slope time allowing the current to reach selected value, pulse duration to allow the arc action and down slope time for the current to drop. As per the pilot experimental results, peak current and pulse duration were the most influential parameters. Similar to ultrasonic and resistance spot welding, micro-TIG welding also exhibited comparatively better strength and bonding when copper was the upper sheet and aluminium was the lower sheet when joining dissimilar materials. Tables 6 and 7 summarise the parameters used for joining different stack-up combinations.

Table 7 Key controlling process parameters used for joining of tab materials using pulsed TIG spot welding

Stack-up combination				Current (A)		Pulse duration (ms)	
Upper material	Thick-ness (mm)	Lower material	Thick-ness (mm)	Value	Suitable range	Value	Suitable range
				Al	0.2	Al	0.2
Al	0.3	Al	0.3	120	110–130	30	25–35
Cu[Ni]	0.2	Cu[Ni]	0.2	140	130–150	55	45–65
Cu[Ni]	0.3	Cu[Ni]	0.3	200	180–200	125	110–135
Cu[Ni]	0.2	Al	0.2	155	140–165	18	15–23
Cu[Ni]	0.3	Al	0.3	196	180–200	56	50–60

3 Results and discussion

Joint strength analysis was conducted based on lap shear and T-peel test results. The following section summarises the results for each joining process including the main failure modes of each joint type.

3.1 Ultrasonic metal welding

In general, tab-to-tab joints formed by ultrasonic metal welding are preferable due to their strength and weldability of similar and dissimilar materials. Figure 9 shows the maximum mean load of lap shear and T-peel tests for each stack-up combination. In the case of ultrasonic metal welding, lap shear joints exhibit a nearly four times higher mean load than the T-peel test. For example, the average loads obtained from the 0.3-mm-thick Cu[Ni]-to-Cu[Ni] joints were 966.78 N and 234.04 N from the lap shear and T-peel tests, respectively. In general, ultrasonic energy produces oscillating shear between the mating surfaces which generates heat breaking the oxide/contamination, and further, produces an atomic bond at elevated temperature. At lower level, the ultrasonic energy is not sufficient to create atomic diffusion bonds across the mating surface resulting in under-weld [31]. In contrast, excessive ultrasonic energy produces

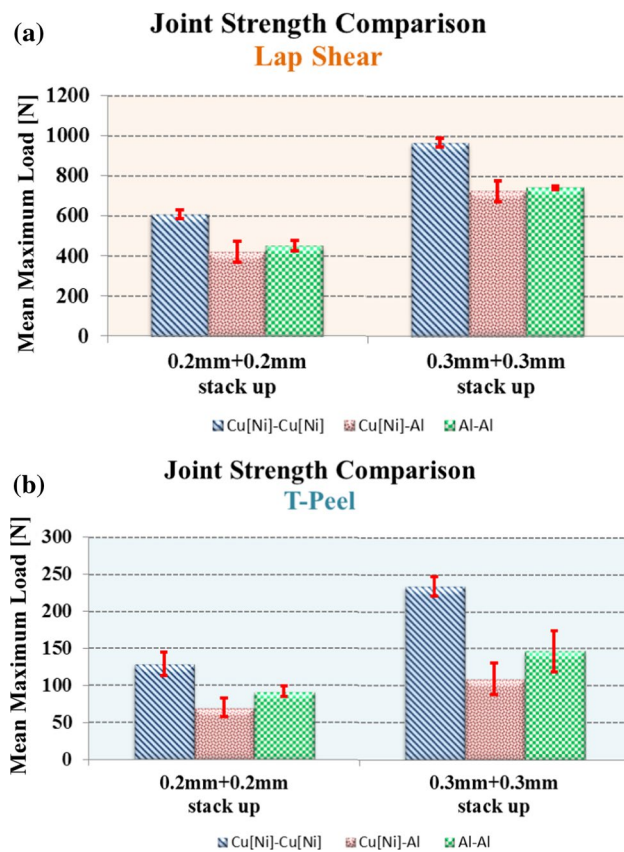
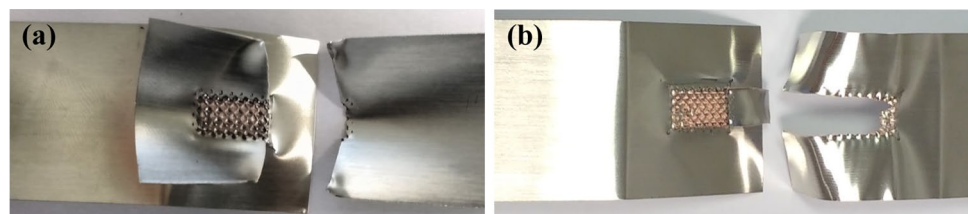


Fig. 9 Joint strength comparison of ultrasonic welded specimen for **a** lap shear, and **b** T-peel tests

ductile flow of materials, high deformation and unnecessary thinning which results in over-weld. A good weld can be achieved by preferred application of ultrasonic energy to the joint which exhibits a strong adhesion without the presence of a gap at the interface [32].

It is also worth noting that the joint strength for dissimilar materials (i.e. Cu[Ni]-to-Al) is relatively lower than that of similar materials (i.e. Cu[Ni]-to-Cu[Ni] or Al-to-Al) for both stack-ups and test types (i.e. lap shear and T-peel). Typical failure modes occurring during lap shear and T-peel tests are shown in Fig. 10. The primary failure for lap shear specimens is material failure around the perimeter of the weld and crack propagation across the width of the specimen. T-peel test specimens exhibit primary failure around the perimeter of the weld and then tearing of the parent material.

Fig. 10 Failure modes of ultrasonic welded Cu[Ni]-to-Cu[Ni] of 0.3-mm-thickness specimens for **a** lap shear, and **b** T-peel tests



3.2 Resistance spot welding

Unlike ultrasonic metal welding, weld nugget size varies for resistance spot welding depending on the diameter of electrode, material stack-up and the current conditions. In case of the resistance spot welding, peak current and peak time are the most important parameters. When the low current is passed through the RSW electrode, the mating surface contact resistance-based heat generation is not sufficient to perform localised melting and subsequent fusion. In contrast, when joining materials are exposed to excessive current for longer peak time, it creates overheating and vaporisation of materials. A balanced peak time to allow the welding at allowable peak current can produce good resistance spot welded joints. During the experimental trials, it was observed that the weld nugget sizes were in the range from 0.9 to 2.0 mm in diameter for different RSW parameters. Furthermore, due to the small weld nugget size, the lap shear and T-peel strengths were comparatively low. Figure 11 displays the maximum mean load of lap shear and T-peel tests for each stack-up combination joined by resistance spot welding. Firstly, it is worth noting that lap shear and T-peel loads for 0.3 mm Cu[Ni] to 0.3 mm Cu[Ni] are lower than the dissimilar materials combination (i.e. 0.3 mm Cu[Ni] to 0.3 mm Al) or 0.2 mm Cu[Ni] to 0.2 mm Cu[Ni] stack-up. This is due to the fact that the heat generated in the thicker copper-to-copper stack-up during welding was conducted away from the welding point and the produced joint nugget was correspondingly smaller. In spite of using a dual-pulse and higher peak current, the joint was still relatively weak. The nugget sizes of resistance spot welded specimens of 0.3-mm-thickness material stack-ups (i.e. Cu[Ni]-to-Cu[Ni], Cu[Ni]-to-Al and Al-to-Al) from lap shear tests were visually inspected and are reported in Fig. 12. It is evident from Fig. 12 that the nugget size for dissimilar material combinations (i.e. Cu[Ni]-to-Al of 0.3 mm thickness) is comparatively larger than that obtained from similar materials combinations (i.e. Cu[Ni]-to-Cu[Ni] and Al-to-Al). Therefore, resistance spot welding exhibits comparatively good joint strength for dissimilar material combinations. For example, 0.3 mm Cu[Ni] to 0.3 mm Al joints show a maximum mean load of 173.1 N and 43.37 N for lap shear and T-peel tests, respectively. It can also be seen that Al-to-Al joints exhibit relatively low strength. Figure 13 shows the typical main failure modes of resistance spot welded joints during

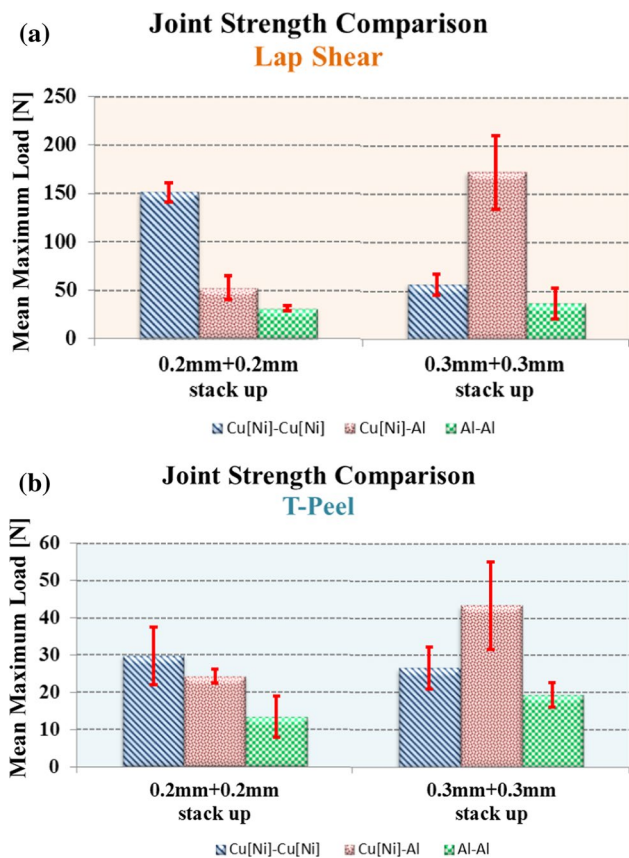


Fig. 11 Joint strength comparison of resistance spot welded specimen for a lap shear, and b T-peel tests

lap shear and T-peel tests. Generally, the failure modes are welding zone failures with circumferential fracture, cracking around the weld nugget followed by material tearing.

3.3 Pulsed TIG spot welding

Pulsed TIG spot welding shows similar load behaviour to resistance spot welding and is able to create joints of strength greater than those made by RSW for thicker Cu[Ni]-to-Cu[Ni] (of 0.3 mm thickness). In case of pulsed TIG spot welding, current and pulse duration are the most important joining process parameters. Weld nugget diameter also varies with peak current and pulse duration; an increase in pulse duration generally results in the nugget size increasing. However, this does not necessary represent an incremental increase in joint strength. It was also observed that longer pulse durations result in material vaporisation, burn-through, and subsequently, weaker joints. From Fig. 14, it can be seen that for 0.3-mm gauge materials the joint strength of specimens comprised of different materials, i.e. Cu[Ni] and Al, is greater than that of joints of the same specimen configuration comprising similar, i.e. Cu[Ni]-to-Cu[Ni] or Al-to-Al, materials. This behaviour may be related to additional heat conduction by more conductive copper materials (i.e. Cu[Ni]-to-Cu[Ni] joint), resulting in smaller nugget size than the Cu[Ni]-to-Al joint. Figure 15 shows the visual inspection of nugget sizes based on pulsed TIG spot welded failure modes from lap shear samples of 0.3 mm to 0.3 mm stack-ups of Cu[Ni]-to-Cu[Ni], Cu[Ni]-to-Al and Al-to-Al. It can be seen that the nugget size of Cu[Ni]-to-Cu[Ni], of 0.3 mm thickness, is relatively small compared with the nugget size of Cu[Ni]-to-Al. Figure 16 shows the typical failure modes associated with pulsed TIG spot welded joints during lap shear and T-peel tests. Similar to resistance spot welding, the failure modes are welding zone cracking and circumferential fractures leading to material tearing.

Fig. 12 Visual inspection of nugget sizes for lap shear tests of resistance spot welded specimens of Cu[Ni]-to-Cu[Ni], Cu[Ni]-to-Al and Al-to-Al (of 0.3 mm thickness)

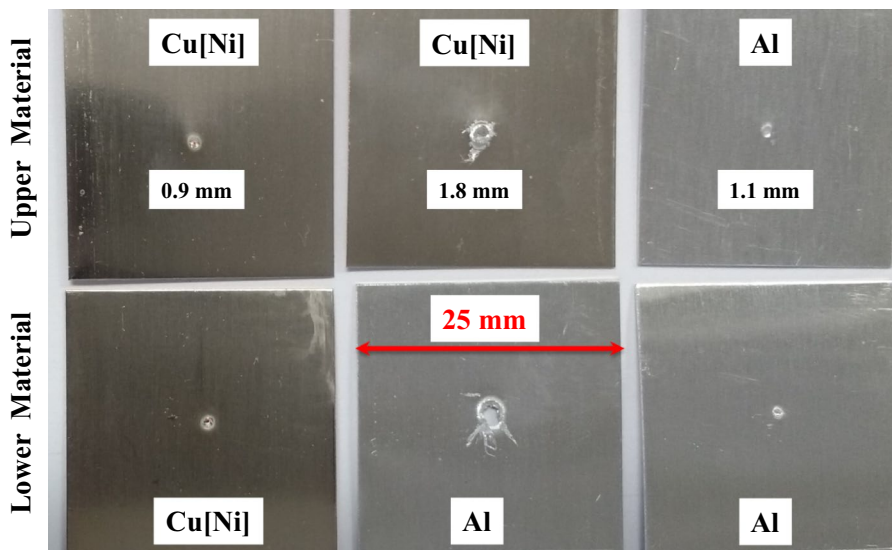


Fig. 13 Failure modes of resistance spot welded Cu[Ni]-to-Cu[Ni] of 0.2-mm-thickness specimens from **a** lap shear, and **b** T-peel tests

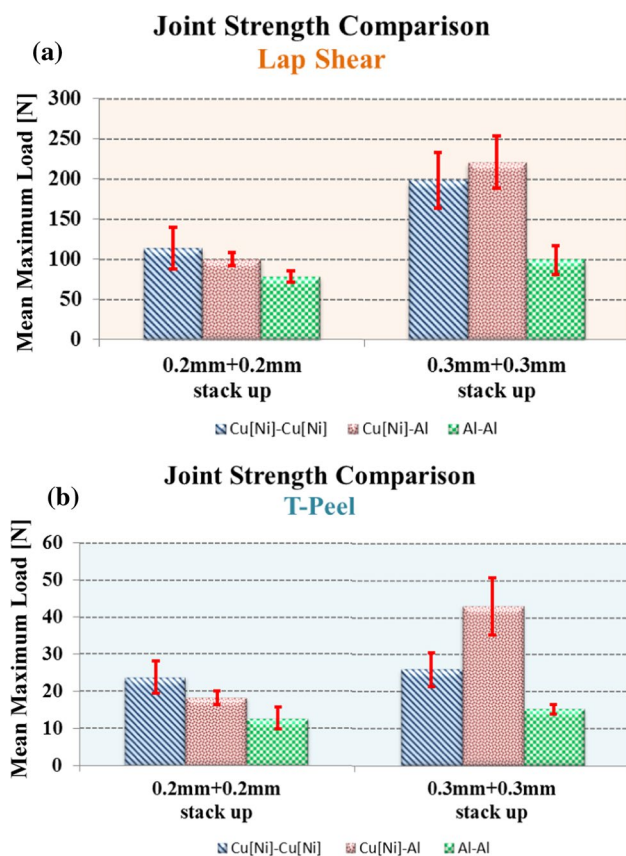
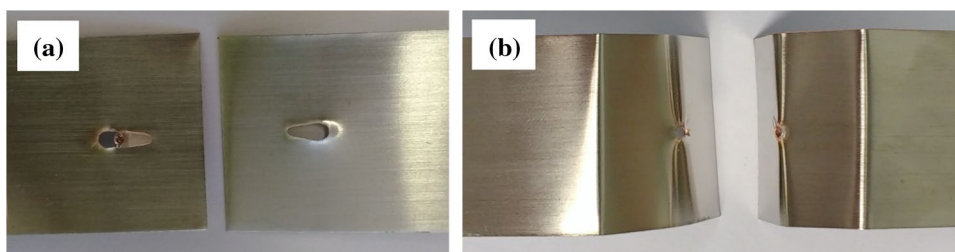


Fig. 14 Joint strength comparison of pulsed TIG spot welded specimen for **a** lap shear, and **b** T-peel

3.4 Strength reduction ratio-based comparison

A strength reduction ratio, as defined in Eq. (1), was employed to provide an indication of the difference in strength of lap shear and T-peel specimen configurations of joining methods. It provides an additional tool for basic comparison between the joining methods, without involving detailed metallographic sectioning and analysis, especially suitable for initial process development phase. Figure 17 exhibits the strength reduction ratio of similar and dissimilar material joints of two stack-ups (i.e. 0.2 mm + 0.2 mm and 0.3 mm + 0.3 mm stack-ups) using ultrasonic metal welding, resistance spot welding and pulsed TIG spot welding. A target value of strength reduction ratio can be set by user

(e.g. process development engineers or quality practitioners) such that joints exhibit equal or higher than the target value (i.e. strength reduction ratio \geq target value) will be accepted for further process optimisation which will eventually lead to candidate technology selection for joining application. For instance, it can be assumed that a strength reduction ratio of 0.8 or higher will be selected for further process optimisation and other quality inspection, such as metallographic sectioning. Based on this target value for the strength reduction ratio, it can be observed that ultrasonic welding exhibited its ability to produce joints with acceptable strengths for joining both thickness stack-ups and all material combinations. In addition, ultrasonic welding has greater capability for joining dissimilar materials. In contrast, resistance spot welding gives a lower strength reduction ratio which indicates it is comparatively less capable for the joint configurations investigated when joining highly conductive materials and warrants in-depth investigations for further improvement. Pulsed TIG spot welding also exhibited its ability to join both similar and dissimilar conductive materials by satisfying the strength reduction ratio criterion. This suggests that based on joint strength and strength reduction ratio alone, pulsed TIG spot welding should be considered as a candidate joining technology for electrical interconnects in battery pack manufacture and supports the need for more detailed investigation for joining process development.

4 Conclusions and final remarks

This paper focuses on mechanical strength characterisation of tab-to-tab joints which are generally used for pouch cell connections. The most commonly used tab materials, aluminium (Al) and nickel-coated copper (Cu[Ni]) of two thicknesses (i.e. 0.2 mm and 0.3 mm), were used for experimental investigations. Overlap joints were created using ultrasonic metal welding, resistance spot welding and pulsed TIG spot welding which are suitable for pouch cell-to-cell connection during battery pack manufacturing. Ultrasonic and resistance spot welding techniques are in current industrial use, whereas pulsed TIG spot welding shows potential for joining of tab materials. The strength of joints made between similar and dissimilar materials, a combination of copper and aluminium, was determined by performing tensile tests

Fig. 15 Visual inspection of nugget sizes for lap shear tests of pulsed TIG spot welded specimens of Cu[Ni]-to-Cu[Ni], Cu[Ni]-to-Al and Al-to-Al (of 0.3 mm thickness)

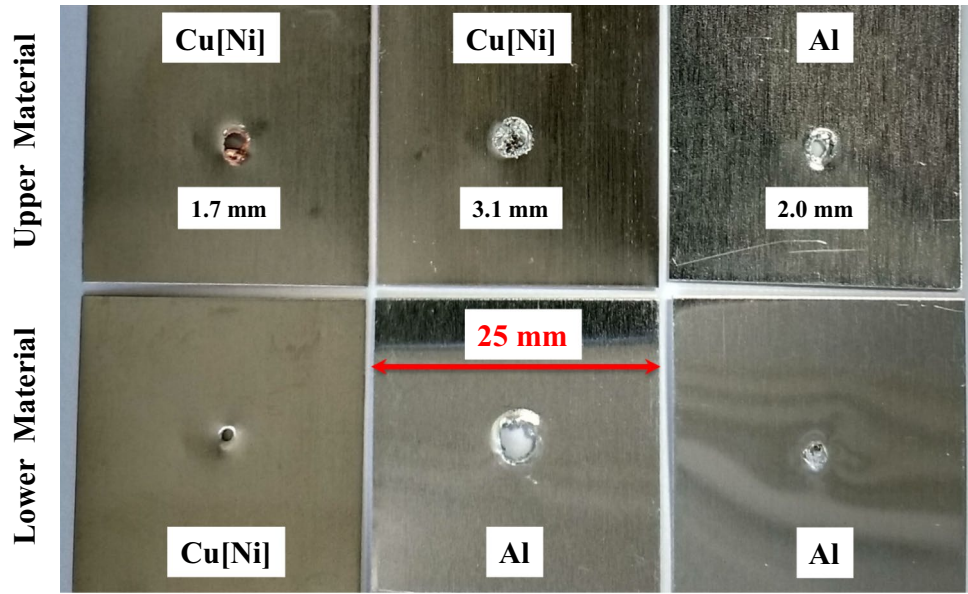


Fig. 16 Failure modes of pulsed TIG spot welded specimens for **a** lap shear (Al-to-Al of 0.2 mm thickness), and **b** T-peel (Cu[Ni]-to-Al of 0.2 mm thickness) tests

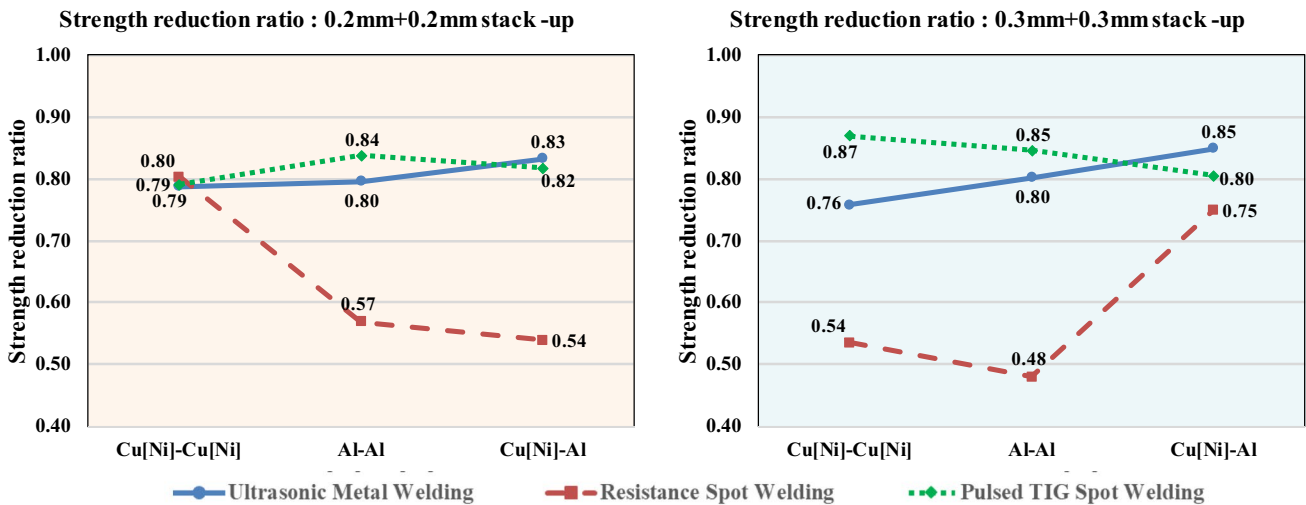
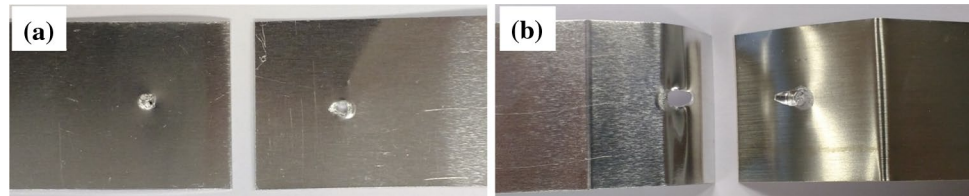


Fig. 17 Strength reduction ratio of similar and dissimilar material joints using ultrasonic metal welding, resistance spot welding and pulsed TIG spot welding

of lap shear and T-peel specimens. The results of these tests are reported.

- When welding dissimilar materials (i.e. Cu[Ni] and Al), it was observed for all the three joining processes that

Cu[Ni] was preferred as the upper sheet and Al as the lower sheet as this combination gave a better result.

- The influencing joining process parameters (e.g. ultrasonic energy for ultrasonic metal welding, peak current and peak time for resistance spot welding, and peak cur-

rent and pulse duration for pulsed TIG spot welding) have been identified in this feasibility study.

- The challenges and issues related to each joining method and influencing process parameters are summarised with failure modes of lap shear and T-peel test specimens, and their load behaviour with ranges are reported.
- A strength reduction ratio is developed in this paper and provides an indication of capability based on strengths achieved by joining methods. The test results provide a basis for selection of joining processes based on mechanical performance of joints for the manufacture of battery modules and packs.

Further work could take advantage of the reported results for joint strength characterisation and consider tab-to-busbar connections and an analysis of fatigue behaviour.

Acknowledgements This research is funded by EPSRC Institutional Grant for the APC Spoke. Resources for experimental trials and testing were provided by the WMG Centre High Value Manufacturing (HVM) Catapult at The University of Warwick.

Open Access This article is distributed under the terms of the Creative Commons Attribution 4.0 International License (<http://creativecommons.org/licenses/by/4.0/>), which permits unrestricted use, distribution, and reproduction in any medium, provided you give appropriate credit to the original author(s) and the source, provide a link to the Creative Commons license, and indicate if changes were made.

References

1. Commission E (2017) Reducing CO₂ emissions from passenger cars. https://ec.europa.eu/clima/policies/transport/vehicles/cars_en#tab-0-0. Accessed 25-03-2017
2. Das A, Butterworth I, Masters I, Williams D (2018) Microstructure and mechanical properties of gap-bridged remote laser welded (RLW) automotive grade AA 5182 joints. *Mater Charact* 145:697–712. <https://doi.org/10.1016/j.matchar.2018.09.035>
3. Jansen AN, Amine K, Newman AE, Vissers DR, Henriksen GL (2002) Low-cost, flexible battery packaging materials. *JOM* 54(3):29–32. <https://doi.org/10.1007/BF02822616>
4. The Chevy Bolt Battery Pack Possibilities. (2015). <http://gm-volt.com/2015/06/22/the-chevy-bolt-battery-pack-possibilities/>. Accessed 2017-07-05
5. Design Possibilities for the Chevy Bolt. (2015). <http://gm-volt.com/2015/06/19/design-possibilities-for-the-chevy-bolt/>. Accessed 2017-07-05
6. Lu L, Han X, Li J, Hua J, Ouyang M (2013) A review on the key issues for lithium-ion battery management in electric vehicles. *J Power Sources* 226:272–288. <https://doi.org/10.1016/j.jpowsour.2012.10.060>
7. Nitta N, Wu F, Lee JT, Yushin G (2015) Li-ion battery materials: present and future. *Mater Today* 18(5):252–264. <https://doi.org/10.1016/j.mattod.2014.10.040>
8. Deng D (2015) Li-ion batteries: basics, progress, and challenges. *Energy Sci Eng* 3(5):385–418. <https://doi.org/10.1002/ese3.95>
9. Lee SS, Kim TH, Hu SJ, Cai WW, Abell JA (2010) Joining technologies for automotive lithium-ion battery manufacturing: a review. In: ASME 2010 international manufacturing science and engineering conference, Pennsylvania, USA, 2010, pp 541–549
10. Das A, Li D, Williams D, Greenwood D (2018) Joining technologies for automotive battery systems manufacturing. *World Electr Veh J* 9(2):22. <https://doi.org/10.3390/wevj9020022>
11. Elangovan S, Semeer S, Prakasan K (2009) Temperature and stress distribution in ultrasonic metal welding—an FEA-based study. *J Mater Process Technol* 209(3):1143–1150. <https://doi.org/10.1016/j.jmatprotec.2008.03.032>
12. De Vries E (2004) Mechanics and mechanisms of ultrasonic metal welding. The Ohio State University
13. Zhang C, Li L (2009) A coupled thermal–mechanical analysis of ultrasonic bonding mechanism. *Metall Mater Trans B* 40(2):196–207. <https://doi.org/10.1007/s11663-008-9224-9>
14. Das A, Masters I, Williams D (2018) Process robustness and strength analysis of multi-layered dissimilar joints using ultrasonic metal welding. *Int J Adv Manuf Technol*. <https://doi.org/10.1007/s00170-018-2936-3>
15. Siddiq A, Ghassemieh E (2008) Thermomechanical analyses of ultrasonic welding process using thermal and acoustic softening effects. *Mech Mater* 40(12):982–1000. <https://doi.org/10.1016/j.mechmat.2008.06.004>
16. Kim TH, Yum J, Hu SJ, Spicer JP, Abell JA (2011) Process robustness of single lap ultrasonic welding of thin, dissimilar materials. *CIRP Ann Manuf Technol* 60(1):17–20. <https://doi.org/10.1016/j.cirp.2011.03.016>
17. Shawn Lee S, Hyung Kim T, Jack HuS, Cai WW, Abell JA, Li J (2013) Characterization of joint quality in ultrasonic welding of battery tabs. *J Manuf Sci Eng* 135(2):021004–021013. <https://doi.org/10.1115/1.4023364>
18. Kang B, Cai W, Tan C-A (2014) Dynamic stress analysis of battery tabs under ultrasonic welding. *J Manuf Sci Eng* 136(4):041011. <https://doi.org/10.1115/1.4026990>
19. Bergmann JP, Regensburg A, Schürer R, Petzoldt F, Herb A (2017) Effect of the interface characteristics on the joint properties and diffusion mechanisms during ultrasonic metal welding of Al/Cu. *Weld World* 61(3):499–506. <https://doi.org/10.1007/s40194-017-0449-6>
20. Brand MJ, Schmidt PA, Zaeh MF, Jossen A (2015) Welding techniques for battery cells and resulting electrical contact resistances. *J Energy Storage* 1:7–14. <https://doi.org/10.1016/j.est.2015.04.001>
21. Chang B, Zhou Y (2003) Numerical study on the effect of electrode force in small-scale resistance spot welding. *J Mater Process Technol* 139(1):635–641
22. Matsushita M, Ikeda R, Oi K (2015) Development of a new program control setting of welding current and electrode force for single-side resistance spot welding. *Weld World* 59(4):533–543. <https://doi.org/10.1007/s40194-015-0228-1>
23. Dong S, Kelkar G, Zhou Y (2002) Electrode sticking during micro-resistance welding of thin metal sheets. *IEEE Trans Electron Packag Manuf* 25(4):355–361
24. Micro TIG Welding. Amada Miyachi, Inc. <http://www.amada-miyachi.com/products/micro-tig>. Accessed 2017-07-06
25. Hirata Y (2003) Pulsed arc welding. *Weld Int* 17(2):98–115. <https://doi.org/10.1533/wint.2003.3075>
26. Shakil M, Tariq NH, Ahmad M, Choudhary MA, Akhter JI, Babu SS (2014) Effect of ultrasonic welding parameters on microstructure and mechanical properties of dissimilar joints. *Mater Des* 55:263–273. <https://doi.org/10.1016/j.matdes.2013.09.074>
27. Zhou Y, Gorman P, Tan W, Ely KJ (2000) Weldability of thin sheet metals during small-scale resistance spot welding using an alternating-current power supply. *J Electron Mater* 29(9):1090–1099. <https://doi.org/10.1007/s11664-004-0270-z>

28. Park M, Hirata Y (2017) Research on generation of micro-plasma arc and its power intensity. *Weld Int* 31(4):284–290. <https://doi.org/10.1080/09507116.2016.1223214>
29. Yang M, Yang Z, Qi B (2015) The effect of pulsed frequency on the plasma jet force with ultra high-frequency pulsed arc welding. *Weld World* 59(6):875–882. <https://doi.org/10.1007/s40194-015-0261-0>
30. Han L, Thornton M, Shergold M (2010) A comparison of the mechanical behaviour of self-piercing riveted and resistance spot welded aluminium sheets for the automotive industry. *Mater Des* 31(3):1457–1467. <https://doi.org/10.1016/j.matdes.2009.08.031>
31. Gencsoy H, Adams J, Shin SJU (1967) On some fundamental problems in ultrasonic welding of dissimilar metals: Gencsoy, HT, Adams, JA and Shin S. *Welding journal*, 46, no. 4, p. 145-s (1967) 5(4):274
32. Satpathy MP, Moharana BR, Dewangan S, Sahoo SK (2015) Modeling and optimization of ultrasonic metal welding on dissimilar sheets using fuzzy based genetic algorithm approach. *Eng Sci Technol Int J* 18(4):634–647. <https://doi.org/10.1016/j.jestch.2015.04.007>